



**Titre:** Manning's roughness coefficient determination in laboratory experiments using 2D modeling and automatic calibration

**Auteurs:** Basile Lavoie, & Tew-Fik Mahdi

**Date:** 2020

**Type:** Article de revue / Article

**Référence:** Lavoie, B., & Mahdi, T.-F. (2020). Manning's roughness coefficient determination in laboratory experiments using 2D modeling and automatic calibration. [Détermination du coefficient de rugosité de Manning dans des expériences de laboratoire utilisant la modélisation 2D et l'étalonnage automatique]. La Houille Blanche, 106(1), 22-33. <https://doi.org/10.1051/lhb/2020001>

 **Document en libre accès dans PolyPublie**  
Open Access document in PolyPublie

**URL de PolyPublie:** <https://publications.polymtl.ca/5316/>

**Version:** Version finale avant publication / Accepted version  
Révisé par les pairs / Refereed

**Conditions d'utilisation:** Tous droits réservés / All rights reserved

 **Document publié chez l'éditeur officiel**  
Document issued by the official publisher

**Titre de la revue:** La Houille Blanche (vol. 106, no. 1)

**Maison d'édition:** EDP Sciences

**URL officiel:** <https://doi.org/10.1051/lhb/2020001>

**Mention légale:** ©2020. This is the author's version of an article that appeared in La Houille Blanche (vol. 106, no. 1) . The final published version is available at <https://doi.org/10.1051/lhb/2020001>

# Manning's Roughness Coefficient Determination in Laboratory Experiments Using 2D Modeling and Automatic Calibration

Basile Lavoie<sup>(1)</sup>, Tew-Fik Mahdi<sup>(2)</sup>

<sup>(1)</sup> Département des génies Civil, Géologique et des Mines (CGM), École Polytechnique de Montréal, C.P. 6079, succursale Centre-Ville, Montréal, QC H3C 3A7, Canada. Email: basile.lavoie@polymtl.ca

<sup>(2)</sup> Professor, Département des génies Civil, Géologique et des Mines (CGM), École Polytechnique de Montréal, C.P. 6079, succursale Centre-Ville, Montréal, QC H3C 3A7, Canada (Corresponding author). Email: tewfik.mahdi@polymtl.ca

*Reliable experimental data are essential for choosing and validating numerical models. Although numerous data sets have been presented in the literature, few have been made widely available to the scientific community. Additionally, these experimental data sets have generally given little attention to the determination of Manning's Roughness coefficients. This paper addresses these two issues. Three channel configurations are studied: a flatbed channel, a channel with a triangular sill and a channel with a triangular abutment. Three increasing permanent discharges are used for each configuration, leading to nine test cases. The Manning's coefficients are determined using three methods: the traditional step method, automatic calibration, via a 2D hydrodynamic model, considering theoretical value intervals and automatic calibration ignoring these intervals. The results show that automatic calibration with theoretical value intervals is advantageous compared to the step method. Automatic calibration ignoring theoretical intervals yields low errors but unphysical values; therefore, it is not recommended.*

## Key words:

*Laboratory experiment, 2D flow modeling, PEST and SRH-2D, Automatic calibration, Triangular sill and abutment*

## Détermination du coefficient de rugosité de Manning dans des expériences de laboratoire utilisant la modélisation 2D et l'étalonnage automatique

*Des données expérimentales fiables sont essentielles pour choisir et valider des modèles numériques. Bien que de nombreux ensembles de données aient été présentés dans la littérature, peu ont été largement diffusés auprès de la communauté scientifique. De plus, ces ensembles de données expérimentales ont généralement accordé peu d'attention à la détermination des coefficients de rugosité de Manning. Cet article aborde ces deux aspects. Des essais au laboratoire en écoulement permanent dans un canal sont réalisés. Pour ce canal, trois configurations sont étudiées: un canal à fond plat, un canal à fond plat avec un seuil triangulaire à l'aval et un canal à fond plat avec une butée triangulaire. Trois débits de valeurs croissantes sont utilisés pour chaque configuration, conduisant à neuf cas de tests. Les coefficients de Manning sont déterminés à l'aide de trois méthodes: la méthode classique des tronçons, la calibration automatique, en utilisant un modèle hydrodynamique 2D, prenant en compte les intervalles de valeurs théoriques des coefficients de Manning selon la nature des parois du canal, et la calibration automatique ignorant ces intervalles. Les résultats montrent que la calibration automatique prenant en compte les intervalles de valeurs théoriques des coefficients de Manning fournit de meilleurs résultats que la méthode des tronçons. L'étalonnage automatique ignorant les intervalles théoriques produit des erreurs faibles mais des valeurs pour les coefficients de Manning qui ne correspondent pas aux valeurs du matériau du canal; par conséquent, cette dernière méthode n'est pas recommandée. Par ailleurs, l'ensemble des données expérimentales sont fournies avec le présent article. Ces données peuvent être utilisées, sans aucune responsabilité des auteurs, sous réserve que le présent article est cité comme référence.*

## Mots-clefs:

*Expériences de laboratoire, Modélisation 2D, PEST et SRH-2D, Calibration automatique, Seuil et butée triangulaires*

## I INTRODUCTION

Numerical modeling is becoming increasingly interesting for hydraulic engineers because of its speed and ease of use. Available numerical models are numerous; therefore, reliable experimental data sets are needed that allow for model validation and choice of a specific model.

53 This paper presents the production of a data set via the steps encountered in laboratory  
54 experimentation and data processing. Experiments in the hydraulic laboratory of the *École*  
55 *Polytechnique de Montréal* use three channel configurations, in which three increasing permanent  
56 discharges are studied, for a total of nine cases. The three configurations include a flatbed channel,  
57 a channel with triangular sill, and a channel with a triangular abutment.

58 Particular attention is paid to the determination of the Manning's roughness coefficient. Several  
59 methods have been proposed to determine this parameter (Chow 1959; French 1987; Henderson  
60 1966):

- 61 1. The Soil Conservation Service Method, in which a basic coefficient is modified by  
62 correction factors
- 63 2. The use of theoretical tables
- 64 3. The photographic method, in which the channel is compared to other channels with  
65 known resistance values
- 66 4. Velocity measurements
- 67 5. The use of empirical formulas relating Manning's coefficient to bed material size
- 68 6. Measurement of water levels and calculation of energy slopes (step method or energy  
69 slope method)

70 The last method remains the most commonly used for experimentation in laboratory channels. As  
71 part of this study, this method is compared to a new method, automatic calibration, with or without  
72 regard to theoretical values. Automatic calibration is used in hydrologic and hydrodynamic studies  
73 (Ellis et al. 2009; Fabio et al. 2010; McCloskey et al. 2011; Wasantha Lal. 1995; Lin et al. 2017),  
74 but this is the first time, to the authors' knowledge, that it has been applied to retrieve Manning's  
75 roughness coefficients in a laboratory experiment with two-dimensional numerical model. The  
76 previous calibration works are mostly one-dimensional numerical models or calibrations that use  
77 few measurement points. The present study proposes to use automatic calibration with a two-  
78 dimensional model and with a very high density of water depth measurements; from 24 to 30  
79 locations in a 6.7m x 0.762 m channel. This high density is very challenging in the search of an  
80 optimum for the automatic calibration tool and is therefore a good validation of the applicability of  
81 automatic calibration.

82 Moreover, the energy slope method which is usually used to determine the Manning's roughness  
83 coefficients in laboratory experiments is one-dimensional. It has been underlined (Morvan et al,  
84 2010) that roughness coefficients may differ depending on the type of numerical model used, i.e.  
85 one-dimensional or two-dimensional models. Therefore, the use of a one-dimensional method to  
86 determine a coefficient that will be used in 2D modeling might not be the most appropriate way to  
87 proceed. Automatic calibration has the advantage of preventing that possible loss of precision.

88 As presented above, this article aims at two objectives:

- 89 1. Creation and distribution of a dataset to be used in validation of two-dimensional  
90 numerical models.
- 91 2. Validation of automatic calibration with 2D numerical modeling and presentation of  
92 a methodology to determine Manning's Roughness Coefficients in 2D experimental flows.

93 After a brief review of the available experimental data sets for numerical model validation, the  
94 paper details the experimental setup. The testing procedure is then covered, after which the various  
95 calculations necessary to identify Manning's roughness coefficients values are discussed. The  
96 results are then presented and described in order to be used as test cases to validate numerical  
97 models. Finally, concluding remarks and various recommendations are made.

## 99 II BACKGROUND

100 For numerical models' validation, on one hand, several researchers developed analytical solutions  
101 for simple cases. Goutal and Maurel (1997) and Delestre et al. (2013) reviewed most of these

102 solutions such as the ones proposed by Ritter (1892), Stoker (1957), Dressler (1954), Whitham  
103 (1955), Thacker (1981) and MacDonald et al. (1997). On the other hand, many researchers have  
104 participated in the creation and distribution of experimental data. These data sets are typically used  
105 for 1D, 2D or 3D numerical model validation. Two real data sets, the Malpasset test case (Alcrudo  
106 and Gil, 1999; Hervouet and Petitjean, 1999) and the Toce case (Valiani et al., 1999) were  
107 presented during the 4<sup>th</sup> CADAM workshop.

108 In recent years, considerable efforts have focused on experimental and numerical modeling of  
109 transient dam-break flows. [Ozmen-Cagatay and Kocaman \(2011\)](#) simulated a dam break on a  
110 horizontal bed with a trapezoidal sill and used it to compare the Reynolds-Averaged Navier Stokes  
111 and Shallow-Water equations using the CFD software Flow-3D. Similar experiments were  
112 conducted by [Ozmen-Cagatay and Kocaman \(2010\)](#) and [LaRocque et al. \(2013\)](#). [Aureli et al. \(2008\)](#)  
113 modeled a dam break with laboratory experiments and a finite volume code. [Oertel and Bung](#)  
114 [\(2012\)](#) used the observations of a dam break to validate the volume of fluid method (VOF). [Soares-](#)  
115 [Frazão \(2007\)](#) modeled this type of flow along a horizontal bed with a triangular sill and then  
116 against an isolated obstacle (Soares-Frazão and Zech 2007). [Soares-Frazão and Zech \(2008\)](#) and  
117 [Testa et al. \(2007\)](#) finally studied dam-break waves in idealized urban situations.

118 The flow around an abutment has also been given some attention. [Duan \(2009\)](#) studied the three-  
119 dimensional turbulent flow created around a spur dike by measuring its velocity field. [Dey and](#)  
120 [Barbhuiya \(2005\)](#) performed a similar experiment around a rectangular abutment.

121 Although all of these data sets and experiments can be effectively used to validate numerical  
122 methods and improve the understanding of the associated phenomena, careful observations raise the  
123 issue of determining Manning's roughness coefficient. Indeed, the calculation of this parameter is  
124 given relatively little attention and is never clearly explained. It is generally derived from previous  
125 experiences. This is surprising, given that it is mentioned as one of the most influential parameters  
126 in the final solutions of numerical simulations (Warmink et al. 2010). Also note that these data sets  
127 are not always made available to the scientific community; however, this issue is of great  
128 importance considering the proliferation of numerical models and the need for subsequent  
129 validation.

130 These two observations motivate this paper, which emphasizes calculating the Manning's  
131 roughness coefficient and providing reliable and high-quality data.

### 133 III EXPERIMENTAL SETUP

#### 134 III.1 Instrumentation

135 Geometric levels and water depth measurements are carried out using an ultrasonic  
136 mic+340/DIU/TC sensor with an operating range of 350 to 5000 mm and an accuracy of 1%  
137 (Microsonic 2015). The flow is measured with a MAG 910E electromagnetic flowmeter, which can  
138 be applied to any conductive liquid flow (OmniInstruments 2015). The accuracy of the device is 1%  
139 for the range of flow rates used.

#### 140 III.2 Channel Configurations

141 Three different channel configurations are used in this study. All of them were built in the  
142 Hydraulic Laboratory at École Polytechnique de Montréal. We use a rectangular flatbed channel  
143 with a steel bottom and glass walls, which is successively modified by adding a triangular sill and a  
144 triangular abutment. These modifications aim to gradually create a more complex flow. The initial  
145 geometry and the two modifications are described hereafter.

### 146 *III.2.1 First Configuration – Initial Flatbed Channel*

147 The initial channel is composed of glass walls and a steel flatbed. The zone where the flow is  
148 studied is identified in Figure 1. It has a length of 6.70 m, a width of 0.762 m and a depth of 0.764  
149 m. Two cracks of equal dimensions are present in both channel walls at a distance of 0.882 m from  
150 the inlet boundary (figure 2), and they add a two-dimensional component to the flow. These cracks  
151 were used to support a weir in previous experiments.

152 The channel is relatively old; thus, the bed has been slightly modified over the years by corrosion.  
153 Therefore, a geometric survey is performed in 73 locations, improving the knowledge of the exact  
154 channel profile. Figure 3 shows these points and 24 points where the water depth was also surveyed.  
155 The blue dots represent locations where only the bed elevation is known, and red dots show  
156 locations where both the elevation and the water depth are known. These measures can be easily  
157 imported into any meshing software.

### 158 *III.2.2 Second Configuration – Triangular Sill*

159 The second studied configuration was created by adding a wooden triangular sill in the lower part  
160 of the initial channel. The sill has a length of 0.47 m and an average height of 0.126 m. Its crest is  
161 located 5.57 m downstream of the inlet boundary (Figures 4 and 5). A similar configuration was  
162 used for transient flow by [Soares-Frazaõ \(2007\)](#).

163 The geometrical survey used for the first configuration is upgraded by modifying 10 measurement  
164 points and adding 25 others, which brings the geometrical survey of the second configuration to a  
165 total of 98 points. There are 30 locations where the water depth is also known (Figure 6).

### 166 *III.2.3 Third Configuration – Triangular Abutment*

167 The last channel configuration is created by adding a wooden triangular abutment in the upper  
168 part of the initial channel. The abutment is symmetrical, and it has a maximum width of 0.126 m  
169 and a length of 0.48 m. Its crest is located 2.255 m from the inlet boundary (Figures 7 and 8).

170 The geometrical survey used for that last case is the same as the one presented for the first  
171 configuration. Only the channel boundaries need to be modified to represent the abutment. [Dey and](#)  
172 [Barbhuiya \(2005\)](#) showed that a vertical wall abutment induces a highly three-dimensional velocity  
173 field, which may not be well represented by a two-dimensional model such as SRH-2D, which is the  
174 model used in this study and described in section *Automatic Calibration – 2D Flow – All*  
175 *Configurations*. Since the effect of the abutment persists downstream, the flow can be considered as  
176 locally three-dimensional and globally two-dimensional. Therefore, the 24 locations where the  
177 water depth is measured are modified and moved downstream of the abutment to capture the two-  
178 dimensional effects and avoid non-representative results in numerical modeling of 3D effects  
179 (Figure 9).

## 180 **III.3 Experimental Setup**

181 Three permanent discharges are used for each configuration presented above, leading to a total of  
182 nine different cases. These are gradually increased and will be referred to as minimum, medium and  
183 maximum discharges. The inflow is controlled through a valve and a flow sensor while the outflow  
184 is a free outfall boundary condition. To ensure steady state flow, experiments only begin after the  
185 sensor reading of the water surface elevation stabilized, which took approximately 10 minutes after  
186 opening the valve. The methodology applied for the geometric, water depth and discharge surveys  
187 are described hereafter.

### 188 *III.3.1 Geometry*

189 The geometry is measured for the three configurations in the locations previously defined in  
190 Figures 3, 6 and 9. The sensor is placed upon a sliding system (Figure 10), which is moved above  
191 the channel to obtain the levels at all determined locations. The sensor takes continuous readings  
192 and is therefore left at the same point for at least 20 seconds, allowing subsequent statistical  
193 validation and a gain in precision. The sensor gives the distance between its location and the one

194 where the level is needed. The level at a particular point is then given by the subtraction of that  
195 distance from the distance of the most distant point, namely, the datum. Because the sensor reacts  
196 poorly to large slopes induced by the triangular sill, the coordinates of the sill are interpolated based  
197 on the height of its crest and the level of the channel bed.

### 198 *III.3.2 Water Depth*

199 Water depths are surveyed using the same method as that used for the geometry. The water depth  
200 is computed by subtracting the distance from the sensor to the water surface and the distance from  
201 the sensor to the channel bed.

### 202 *III.3.3 Discharge*

203 The discharge entering the channel is controlled with a valve and measured by a flow sensor.  
204 Because the water depth is not measured simultaneously, an experiment can last up to an hour;  
205 therefore, the discharge may show small variations over the duration of the experiment. To verify  
206 these variations, discharges are recorded every three minutes and statistically validated after the  
207 experiment.

## 208 **IV STATISTICAL TREATMENT**

209 As previously mentioned, every value is represented by a series of measurements of the same  
210 phenomenon. A statistical treatment is therefore applied to these series to determine the single value  
211 that best represents reality. [Protassov \(2002\)](#) proposed that an experimental value resulting from a  
212 finite number of measurements may be expressed via equations 1 and 2:

$$213 \quad l_{exp} \pm \Delta l = m \pm s_m t_{vp} \quad (1)$$

$$214 \quad s_m = \frac{1}{N(N-1)} \sum_{i=1}^N (l_i - m)^2 \quad (2)$$

215 where  $l_{exp}$  is the experimental average value;  $\Delta l$  is its uncertainty;  $m$  and  $s_m$  are the average and  
216 standard deviation, respectively, of a series of measured values;  $t_{vp}$  is the Student Coefficient;  $N$  is  
217 the number of measurements; and  $l_i$  is a measured value.

218 The following method is applied to the three types of measurements (discharge, water depth and  
219 geometry):

- 220 1. Computation of the experimental average value ( $l_{exp}=m$ ), experimental standard  
221 deviation ( $s_m$ ), number of freedom degrees and Student coefficient ( $t_{vp}$ );
- 222 2. Calculation of uncertainty ( $\Delta l$ ).

223 Changing the datum for every geometry level and water depths requires subtraction, and the sum  
224 of the uncertainty is then used as the final uncertainty. The x- and y-coordinates are measured with  
225 a measuring tape that is fixed on the edge of the channel and marked to ensure that the sensor can  
226 always be moved and positioned at exact desired locations. Half of the smallest measurement level  
227 of the tape is used as the uncertainty. Table 1 shows that the uncertainties are relatively small, with  
228 the highest associated with the x- and y-coordinates. The inflows to which they refer are detailed in  
229 the *Presentation of Data Sets* section, while the water depths and coordinates are given in appended  
230 text files.

231 Experimental repeatability is verified in the channel with an abutment (third configuration), and  
232 all the manipulations and statistical treatments are repeated twice at the medium discharge level.  
233 Measurements are made when the flow-meter indicates a steady discharge at the inlet. Once the first  
234 set of measurements is done, the channel is totally emptied and the process can be repeated. When  
235 compared, the two experiments present very small differences for both the discharge  
236 (RMSE=0.000678 m<sup>3</sup>/s) and water depth (RMSE=0.00022 m, maximum residual=0.00198).

## 237 V DETERMINATION OF MANNING'S ROUGHNESS COEFFICIENTS

238 Manning's roughness coefficient is calculated in three different ways: the one-dimensional step  
239 method (Chow, 1959 and Henderson 1966), automatic calibration considering the theoretical  
240 Manning's value intervals of the channel materials (2D) and automatic calibration ignoring the  
241 theoretical Manning's value intervals of the channel materials (2D). The step method is applied to  
242 the flatbed channel (first configuration) only, and the automatic calibrations are performed for all  
243 three configurations. These methods all consider the minimum discharge. The Manning's roughness  
244 coefficient is then used for medium and maximum discharges. Since the roughness coefficient  
245 varies with the wetted perimeter, there might be a difference between coefficients for the minimum,  
246 medium and maximum discharges and their respective water depths. To use a single coefficient for  
247 all three discharges, we do the hypothesis that with the present configuration, the coefficient  
248 variations are small enough to be neglected. The validity of this hypothesis is verified in the  
249 *Automatic Calibration with Respect to Theoretical Intervals* section where the Manning's  
250 coefficient provided by the calibration for minimum and maximum discharges are found to be very  
251 similar.

### 252 V.1 Instrumentation

253 Manning's coefficient is considered uniform throughout the whole domain of the initial flatbed  
254 channel and the channel with the triangular abutment (configurations 1 and 3), while it is composed  
255 of two materials for the channel with a wooden triangular sill (configuration 2). These materials are  
256 represented based on the Manning's coefficient intervals proposed by Chow (1959) for corrugated  
257 metal, wood and glass. Because the main part of the channel is composed of a steel bed with glass  
258 walls, the coefficient intervals are computed from the equivalent Manning's constant equation  
259 (Chaudhry 2008). These intervals are computed for the channel with the triangular sill at a distance  
260 of 1.1 m from the inlet boundary and are also used for the two other configurations. The water depth  
261 varies considerably over the sill ( $h_{min}=h_c=0.017$  m and  $h_{max}=0.20$  m), but it occurs over a very  
262 short distance (0.47 m). Therefore, no equivalent Manning's coefficient is computed for that  
263 location. The Manning's coefficient equation is as follows:

$$264 \quad n_c = \frac{[\sum P_i n_i^{3/2}]^{2/3}}{P^{2/3}} \quad (3)$$

265 where  $n_c$  and  $P$  are the equivalent Manning's roughness coefficient and wetted perimeter of the  
266 whole section, respectively, while  $n_i$  and  $P_i$  are for a subsection associated with a specific material.

267 In the step method, calibration values are verified with the theoretical intervals created by the  
268 maximum and minimum values presented in Table 2. For automatic calibration, these intervals are  
269 used as limiting values.

### 270 V.2 Step Method – 1D Flow – Flatbed Channel

271 This method is only used for the flatbed channel (first configuration) at the minimum discharge.  
272 The Manning's coefficient for the equivalent sections made of steel and glass is first computed with  
273 the step method (Henderson 1966):

$$274 \quad \Delta x = \frac{\Delta E}{J_f - J_e} \quad (4)$$

$$275 \quad J_e = \frac{V^2 n^2}{R_h^{4/3}} \quad (5)$$

276 where  $\Delta x$  is the spatial variation in the x-direction,  $\Delta E$  is the energy variation,  $J_f$  is the bed slope,  
277  $J_e$  is the energy slope and  $R_h$  is the hydraulic radius.

278 We use the minimum discharge in the initial flatbed channel, for which the Manning's coefficient  
 279 is calculated in every section bound by two measured water depths. The hydraulic radius is  
 280 calculated from averaged value of the water depth over a cross-section. When calculated using the  
 281 step method, the Manning's roughness coefficients range from 0.012 to 0.017, with an average  
 282 value of 0.014.

283 Figure 11 presents the difference observed between Manning's roughness coefficient calculated  
 284 with the step method and that recommended by the theory. The calculated coefficients are slightly  
 285 below the theoretical values. This may be explained by the fact that these coefficients were  
 286 determined for one-dimensional flow which is not completely achieved with the flatbed  
 287 configuration. Also theoretical intervals were determined for materials that are not identical to  
 288 those used in this study, such variations are therefore reasonable.

### 289 V.3 Automatic Calibration – 2D Flow – All Configurations

290 Automatic calibration is used to retrieve Manning's roughness coefficients for the three channel  
 291 configurations at the minimum discharge. Three models are used in this paper, including the finite-  
 292 volume code SRH-2D (Lai 2008), the pre-treatment and post-treatment software SMS (AQUAVEO  
 293 2016) and the automatic calibration model PEST (Doherty 2005).

#### 294 V.3.1 SRH-2D

295 SRH-2D solves the shallow-water equations of the following form (Lai 2008).

$$\frac{\partial h}{\partial t} + \frac{\partial hU}{\partial x} + \frac{\partial hV}{\partial x} = e \quad (6)$$

296

$$\frac{\partial hU}{\partial t} + \frac{\partial hUU}{\partial x} + \frac{\partial hVU}{\partial y} = \frac{\partial hT_{xx}}{\partial x} + \frac{\partial hT_{xy}}{\partial y} - gh \frac{\partial z}{\partial x} - \frac{\tau_{bx}}{\rho} \quad (7)$$

297

$$\frac{\partial hV}{\partial t} + \frac{\partial hUV}{\partial x} + \frac{\partial hVV}{\partial y} = \frac{\partial hT_{xy}}{\partial x} + \frac{\partial hT_{yy}}{\partial y} - gh \frac{\partial z}{\partial y} - \frac{\tau_{by}}{\rho} \quad (8)$$

298

299 The friction is determined using the Manning equation:

$$\begin{pmatrix} \tau_{bx} \\ \tau_{by} \end{pmatrix} = \rho C_f \left( \frac{U}{V} \right) \sqrt{U^2 + V^2} \quad (9)$$

300

$$C_f = \frac{gn^2}{h^3} \quad (10)$$

301

302

303 Boussinesq equations are used to compute the turbulent stresses:

$$T_{xx} = 2(\nu + \nu_t) \frac{\partial U}{\partial x} - \frac{2}{3}k \quad (11)$$

304

$$T_{xy} = (\nu + \nu_t) \left( \frac{\partial U}{\partial y} - \frac{\partial V}{\partial x} \right) \quad (12)$$

305

$$T_{yy} = 2(\nu + \nu_t) \frac{\partial V}{\partial y} - \frac{2}{3}k \quad (13)$$

306

307

308 where  $h$  is the water depth,  $u$  and  $v$  are the velocity components,  $e$  is a source term,  $T$  is the  
309 turbulent stress,  $\tau$  is the shear stress,  $g$  is the gravitational acceleration,  $\rho$  is the mass density,  $\mu_0$   
310 is the kinematic viscosity of water,  $\mu_t$  is the turbulent eddy viscosity and  $k$  is the turbulent kinetic  
311 energy.

312 SRH-2D proposes two turbulence models: the k-epsilon and depth-averaged parabolic models.  
313 The k-epsilon model with default parameters values is used in this article.

#### 314 *V.3.2 SMS*

315 The Surface-water Modeling System (SMS; (AQUAVEO 2016) allows the user to execute the  
316 required pre-treatment and post-treatment procedures for hydraulic modeling of open channel flow.  
317 The pre-treatment includes the importation of geometry points, definition of the digital elevation  
318 model, interpolation of elevations via triangulation and creation of mesh. The post-treatment  
319 capabilities include the visualization of results in three-dimensions.

#### 320 *V.3.3 PEST*

321 PEST (Doherty 2005) is a software that performs automatic calibration and sensitivity analysis of  
322 any model based on input and output files in binary or text formats. Only the automatic calibration  
323 module is used in this paper. For the present application, the user first has to set up a normal  
324 simulation with values of elevations, materials and boundary conditions and ensure that this  
325 simulation runs properly. PEST is then used to do and control several runs of the simulation while  
326 varying the calibrated parameter (roughness coefficient) and comparing the results with observation  
327 data (provided by the modeler). At the end of this process, a calibrated parameter that lower the  
328 difference between modeled and observed values of water depth is determined. Automatic  
329 calibration with PEST requires three main types of file: template, instruction and control files. The  
330 template files act as models for PEST when creating input files to calibrate the model (SRH-2D).  
331 Instruction files aid PEST in the interpretation of the model's output by indicating the values that  
332 should be used in the calibration. The control file contains calibration instructions, such as stopping  
333 criteria, and observed values. It relates the template and instruction files to the associated model  
334 files. The process is detailed in figure 12.

#### 335 *V.3.4 Flow Modeling*

336 The meshes are composed of triangular elements with an average side size of 0.05 m. Based on  
337 the channel, meshes have lengths of 6.7 m and widths of 0.762 m. Boundary conditions are applied  
338 as defined in the *Presentation of Data Sets section* and the minimum discharge is used. The  
339 experimental setup presents a channel with a free outfall boundary conditions and therefore a  
340 critical depth. However, the critical depth before a freefall is hard to locate precisely and this would  
341 create some uncertainties for numerical modeling. Instead, the last row of measurements ( $x=6.7$  m)  
342 is averaged to give a mean depth that is utilized as a numerical boundary condition. The total  
343 simulation time is 15 minutes, ensuring that the model reaches a steady flow conditions and that  
344 flow depths do not vary in time, i.e. the water depth do not vary between the two last time step. A  
345 sensitivity analysis has been done previously to determine a time step that ensure a balance between  
346 numerical stability, quality of results and computation time. A time step of 0.1 seconds was found  
347 to be adequate. Figure 13 shows the three meshes used to model and calibrate the three  
348 configurations.

#### 349 *V.3.5 Automatic Calibration with Respect to Theoretical Intervals*

350 Automatic calibration is then performed using theoretical intervals. This method aims to  
351 determine Manning's coefficients that minimize the difference between observed and modeled  
352 water depths, while maintaining values that are physically representative of the real channel. This  
353 method is used for all three channels at the minimum discharge rate. Additionally, all the measured  
354 water depths, except the outflow boundary conditions, are used in the calibration, specifically, 21  
355 locations in the flatbed channel and the channel with the abutment and 27 locations in the channel  
356 with the triangular sill. When computed in this manner, the coefficients lead to an RMSE that is

357 relatively small for configurations 1 and 3 and a bit higher for configuration 2, likely because the  
358 presence of a second material complicates the search for an optimum (Table 3).

359 As stated in section *Determination of Manning's Roughness Coefficients*, the hypothesis was  
360 made that a coefficient calibrated with the minimum discharge could be used with the medium and  
361 maximum discharges. To verify this, automatic calibration of the flatbed channel is also performed  
362 with the maximum discharge and calibrated coefficients for minimum and maximum discharges are  
363 compared. The roughness coefficient determined for the steel/glass compound section and the  
364 maximum discharge is  $0.0176 \text{ s/m}^{1/3}$ . This is very close to the value obtained for the minimum  
365 discharge ( $0.017\text{s/m}^{1/3}$ ). These results support the use of same Manning's coefficients with all  
366 discharges in the present test-cases.

### 367 *V.3.6 Automatic Calibration Ignoring Theoretical Intervals*

368 To evaluate the impacts of the chosen intervals on the results of the PEST calibration, a second  
369 series of calibrations is performed with larger intervals of 0.005 to 0.05 that do not account for the  
370 theoretical values. The Manning's roughness coefficients computed for the flatbed channel and  
371 channel with the triangular abutment are similar to those calculated previously, and their RMSEs  
372 are less than half of the previous values (Table 4). However, the coefficients calculated for the  
373 channel with the triangular sill are very different but have similar RMSEs. Additionally, these  
374 coefficients are inconsistent with the theoretical results because they yield larger roughness values  
375 for the wood, which is contradicted by visual inspection. These results emphasize the importance of  
376 carefully defining the calibration intervals to prevent the model from converging to a non-physical  
377 optimum.

## 378 **V.4 Comparison of Calibration Methods**

379 Figure 14 compares the errors calculated based on the water depths in the flatbed channel when  
380 modeled with SRH-2D via SMS, with Manning's coefficients computed by the three  
381 aforementioned methods. The step method gives the most important RMSE, followed by automatic  
382 calibration with consideration of theoretical intervals. Both are superior to the automatic calibration  
383 that ignores theoretical intervals. However, considering the non-physical values resulting from that  
384 method for the channel with the triangular sill, the automatic calibration with chosen intervals  
385 remains the best method. The fact that automatic calibration with theoretical intervals provides a  
386 smaller RMSE than the step method for the simplest configuration studied, even with a small  
387 difference, supports the ability of this method to retrieve Manning's roughness coefficients.  
388 Therefore, this method becomes particularly applicable for experimental setups where more than  
389 one material is used or setups with two-dimensional flow that are not properly represented by the  
390 step method. The possibility of coupling PEST with any model offers the flexibility to find the  
391 Manning's coefficient of a certain type of flow with the most appropriate model according to the  
392 user's judgement.

## 393 **VI PRESENTATION OF DATA SETS**

394 Table 5 presents a summary of the available data sets for the three channel configurations. For  
395 each configuration, three discharges are available, with corresponding boundary conditions.

396 The boundary conditions include discharge at the inflow boundary and a water depth at the  
397 outflow boundary. The water depth is an average of three measured water depths at the outflow  
398 boundary, specifically, 6.7 m from the inlet. Table 6 shows the final Manning's roughness  
399 coefficients that should be used by the modeler.

400 The results are available in three supplementary data files (*Configuration\_1.pdf*,  
401 *Configuration\_2.pdf*, *Configuration\_3.pdf*). The three files contain three series of water depths, one  
402 for each discharge. All coordinates and water depth values are in SI units.

403 **VII CONCLUSION**

404 This paper presents the acquisition and processing of the geometric and water depth data in nine  
405 flow cases, including three discharges in three channel configurations. These data sets were  
406 statistically processed, and the Manning's coefficients were determined by three different methods:  
407 calculating the energy slope, automatic calibration taking into account the theoretical coefficient  
408 intervals and automatic calibration ignoring these intervals. These three methods are compared, and  
409 it appears that automatic calibration is advantageous if it takes into account the theoretical intervals;  
410 otherwise, the model may converge to a global optimum that is not physically representative of the  
411 situation. The acquired data sets are given in appended text files, and the SMS and SRH-2D files  
412 used are available upon request. Users are invited to use these data sets in their studies with proper  
413 citation of the source.

414 **VIII NOMENCLATURE**

415	e	Source term;
416	g	Gravitational acceleration;
417	h	Water depth;
418	$J_e$	Energy slope;
419	$J_f$	Bed slope;
420	k	Turbulent kinetic energy;
421	$l_{exp}$	Experimental value ("ell");
422	$l_i$	Measured value ("ell");
423	m	Average measured value;
424	N	Number of measurements;
425	n	Manning's roughness coefficient;
426	$n_c$	Equivalent Manning's roughness coefficient;
427	$n_i$	Manning's roughness coefficient of a subsection;
428	P	Wetted perimeter;
429	$R_h$	Hydraulic radius;
430	$s_m$	Standard deviation of a series of measured values;
431	T	Turbulence stress;
432	t	Time;
433	$t_{vP}$	Student coefficient associated with a degree of freedom and probability;
434	u	Velocity component (x-direction);
435	v	Velocity component (y-component);
436	$\Delta E$	Energy variation;
437	$\Delta l$	Uncertainty of an experimental value;
438	$\Delta x$	Spatial variation in the x-direction;
439	$\mu_0$	Kinematic viscosity of water;
440	$\mu_t$	Turbulent eddy viscosity;
441	$\rho$	Mass density;
442	$\tau$	Shear stress.

443 **IX ACKNOWLEDGMENTS AND THANKS**

444 This research was supported in part by a National Science and Engineering Research Council  
445 (NSERC) Discovery Grant, application No: RGPIN-2016-06413.

446 **X REFERENCES**

447 Alcrudo, F. and Gil, E. (1999). The Malpasset dam break case study the 4<sup>th</sup> CADAM Workshop,  
448 Zaragoza, 95-109.

449 AQUAVEO (2016). "SMS 12.1 - The Complete Surface-water Solution."  
450 <<http://www.aquaveo.com/software/sms-surface-water-modeling-system-introduction>>. (March 10,  
451 2016).

452 Aureli, F., Maranzoni, A., Mignosa, P., and Ziveri, C. (2008). "Dam-Break Flows: Acquisition of  
453 Experimental Data through an Imaging Technique and 2D Numerical Modeling." *Journal of*  
454 *Hydraulic Engineering*, 10.1061/(ASCE)0733-9429(2008)134:8(1089), 1089-1101.

455 Chaudhry, H. (2008). *Open-Channel Flow*, Springer Science, New-York.

456 Chow, V. T. (1959). *Open-Channel Hydraulics*, McGraw-Hill, New-York.

457 Delestre, O., Lucas, C., Ksinant, P.-A., Darboux, F., Laguerre, C., Vo, T. N. T., James, F., and  
458 Cordier, S. (2013). SWASHES: a compilation of Shallow-Water analytic solutions for hydraulic  
459 and environmental studies. *International Journal for Numerical Methods in Fluids*, 72:269–300.

460 Dey, S., and Barbhuiya, K. (2005). "Flow Field at a Vertical-Wall Abutment." *Journal of*  
461 *Hydraulic Engineering*, 10.1061/(ASCE)0733-9429(2005)131:12(1126), 1126-1135.

462 Dressler, R. F. (1954). Comparison of theories and experiments for the hydraulic dam-break  
463 wave. *International Association of Sciences Hydrology*, 3 (38), 319–328.

464 Doherty (2005). "PEST, Model-Independent Parameter Estimation, User Manual: 5th Edition."  
465 Watermark Numerical Computing.

466 Duan, J. G. (2009). "Mean Flow and Turbulence around a laboratory Spur Dike." *Journal of*  
467 *Hydraulic Engineering*, 10.1061/(ASCE)HY.1943-7900.0000077, 803-811.

468 Ellis, R. J. I., Doherty, J., Searle, R. D., and Moodie, K. (2009). "Applying PEST (Parameter  
469 ESTimation) to improve parameter estimation and uncertainty analysis in WaterCAST models."  
470 *18th World IMACS/MODSIM Congress*, Modelling and Simulation Society of Australia and New-  
471 Zealand Inc., 3158-3164.

472 Fabio, P., Aronica, G. T., and Apel, H. (2010). "Towards automatic calibration of 2-D flood  
473 propagation models." *Hydrology and Earth System Sciences*, 10.5194/hess-14-911-2010, 911-924.

474 French, R. H. (1987). *Open Channel Hydraulics*, McGraw-Hill Book Company, New-York.

475 Goutal, N. and Maurel, F. (1997). Proceedings of the 2nd workshop on dambreak wave  
476 simulation. Technical Report HE-43/97/016/B, Electricité de France, Direction des études et  
477 recherches.

478 Henderson, F. M. (1966). *Open Channel Flow*, Macmillan Publishing Co., Inc., New-York.

479 Hervouet, J. M. and Petitjean, A. (1999). Malpasset dam-break revisited with two-dimensional  
480 computations *Journal of Hydraulic Research*, 37(6), 777-788.

481 Lai, Y. G. (2008). "SRH-2D version 2: Theory and User's Manual." U.S. Department of the  
482 interior - Bureau of Reclamation, Denver.

483 LaRocque, L. A., Imran, J., and Chaudhry, M. H. (2013). "Experimental and Numerical  
484 Investigations of Two-Dimensional Dam-Break Flows." *Journal of Hydraulic Engineering*,  
485 10.1061/(ASCE)HY.1943-7900.0000705, 569-579.

486 Lavoie, B. and Mahdi, T. (2016). "Comparison of two-dimensional Flood Propagation Models:  
487 SRH-2D and HYDRO\_AS-2D." *Natural Hazards*, 10.1007/s11069-016-2737-7, 1207-1222

488 Lin, F.-R., Wu, N.-J., Tu, C.-H., Tsay, T.-K. (2017). "Automatic Calibration of an Unsteady River  
489 Flow Model by Using Dynamically Dimensioned Search Algorithm." *Mathematical Problems in*  
490 *Engineering*, 10.1155/2017/7919324, 19 pages

491 MacDonald, I., Baines, M. J., Nichols, N. K. and Samuels, P. G. (1997). Analytic benchmark  
492 solutions for open-channel flows *Journal of Hydraulic Engineering*. 123(11), 1041-1045

493 McCloskey, G. L. I. E., R.J., Waters, D. K., and Stewart, J. (2011). "PEST hydrology calibration  
494 process for source catchments - applied to the Great Barrier Reef, Queensland." *19th International*  
495 *Congress on Modelling and Simulation*, Modelling and Simulation Society of Australia and New-  
496 Zealand Inc., 2359-2366.

497 Microsonic (2015). "mic+340/IU/TC." <[http://www.microsonic.de/en/distance-](http://www.microsonic.de/en/distance-sensors/cylindrical/micplus/standard-sensors/standard-sensors/micplus340iutc.htm)  
498 [sensors/cylindrical/micplus/standard-sensors/standard-sensors/micplus340iutc.htm](http://www.microsonic.de/en/distance-sensors/cylindrical/micplus/standard-sensors/standard-sensors/micplus340iutc.htm)>. (March, 12,  
499 2016).

500 Morvan, H., Knight, D., Wright, N., Tang, XN and Crossley, A. (2010). "The concept of  
501 roughness in fluvial hydraulics and its formulation in 1D, 2D and 3D numerical simulation models"  
502 *Journal of Hydraulic Research*, 10,1080/00221686.2008.9521855, 191-208.

503 Oertel, M., and Bung, D. (2012). "Initial stage of two-dimensional dam-break waves: laboratory  
504 versus VOF." *Journal of Hydraulic Research*, 10.1080/00221686.2011.639981, 89-97.

505 OmniInstruments (2015). "MAG 910 Electromagnetic Flowmeter."  
506 <[http://www.omniinstruments.co.uk/flow-meters/electromagnetic-flow-meters-magnetic-flow-](http://www.omniinstruments.co.uk/flow-meters/electromagnetic-flow-meters-magnetic-flow-meters/mag910e-magnetic-flowmeter.html)  
507 [meters/mag910e-magnetic-flowmeter.html](http://www.omniinstruments.co.uk/flow-meters/electromagnetic-flow-meters-magnetic-flow-meters/mag910e-magnetic-flowmeter.html)>. (March, 12, 2016).

508 Ozmen-Cagatay, H., and Kocaman, S. (2010). "Dam break flows during initial stage using SWE  
509 and RANS approaches." *Journal of Hydraulic Research*, 10.1080/00221686.2010.507342, 603-611.

510 Ozmen-Cagatay, H., and Kocaman, S. (2011). "Dam-Break Flow in the Presence of Obstacle:  
511 Experiment and CFD Simulation." *Engineering Applications of Computational Fluid Mechanics*,  
512 10.1080/19942060.2011.11015393, 541-552.

513 Protassov, K. (2002). *Analyse statistique de données expérimentales*, EDP Sciences, Les Ulis.

514 Ritter, A. (1892). Die Fortpflanzung der Wasserwellen. Vereine Deutcher Ingenieure Zeitschrift,  
515 36, 947-954.

516 Soares-Frazão, S. (2007). "Experiments of dam-break wave over a triangular bottom sill." *Journal*  
517 *of Hydraulic Research*, 10.1080/00221686.2007.9521829, 19-26.

518 Soares-Frazão, S., and Zech, Y. (2007). "Experimental study of dam-break flow against an  
519 isolated obstacle." *Journal of Hydraulic Research*, 10.1080/00221686.2007.9521830, 27-36.

520 Soares-Frazão, S., and Zech, Y. (2008). "Dam-break flow through an idealised city." *Journal of*  
521 *Hydraulic Research*, 10.3826/jhr.2008.3164, 648-658.

522 Stoker, J. J. (1957). *Water Waves: The Mathematical Theory with Applications* Interscience  
523 Publishers, New York, USA.

524 Testa, G., Zuccalà, D., Alcrudo, F., Mulet, J., and Soares-Frazão, S. (2007). "Flash flood flow  
525 experiment in a simplified urban district." *Journal of Hydraulic Research*,  
526 10.1080/00221686.2007.9521831, 37-44.

527 Thacker, W. C. (1981). Some exact solutions to the nonlinear shallow-water wave equations.  
528 *Journal of Fluid Mechanics Digital Archive*, 107, 499-508

529 Valiani, A., Caleffi, V. and Zanni, A. (1999). Finite Volume scheme for 2D Shallow-Water  
530 equations: Application to a flood event in the Toce river the 4<sup>th</sup> CADAM Workshop, Zaragoza, 185-  
531 206.

532 Warmink, J. J., Van der Klis, H., Booij, M. J., and Hulscher, S. J. M. H. (2010). "Identification  
533 and Quantification of Uncertainties in a Hydrodynamic River Model Using Expert Opinions."  
534 *Water Resources Management*, 10.1007/s11269-010-9716-7, 601-622.

535 Wasantha Lal, A.M. (1995). "Calibration of Riverbed Roughness." *Journal of Hydraulic*  
536 *Engineering*, 10.1061/(ASCE)0733-9429(1995)121:9(664), 664-671.

537 Whitham, G. (1955). The effects of hydraulic resistance in the dam-break problem. Proc. Roy.  
538 Soc. of London, Ser. A., 227, 399-407

539

540

541

542 **XI TABLES**

**Table 1.** Uncertainties in measured values

Measured value	Maximum uncertainty
Water depth (m)	$3.65 \times 10^{-4}$
Discharge (m <sup>3</sup> /s)	$3 \times 10^{-3}$
X-coordinate (m)	$1 \times 10^{-3}$
Y-coordinate (m)	$1 \times 10^{-3}$
Z-coordinate (m)	$1.3 \times 10^{-4}$

**Table 2.** Theoretical intervals of Manning's roughness coefficient

Material	Minimum value (s/m <sup>1/3</sup> )	Maximum value (s/m <sup>1/3</sup> )
Corrugated metal <sup>a</sup>	0.021	0.030
Wood <sup>a</sup>	0.010	0.014
Glass <sup>a</sup>	0.009	0.013
Equivalent constant Manning – steel/glass	0.017	0.028

<sup>a</sup>Based on Chow (1959)

544

545

**Table 3.** Manning's coefficients determined with automatic calibration for theoretical intervals

Configuration	Manning's Coefficient ( $s/m^{1/3}$ )		Error (m)	
	Steel/Glass	Wood	RMSE	Max. Residual
Flatbed channel	0.0170	-	0.0019	0.0032
Channel with sill	0.0174	0.0140	0.0116	0.0215
Channel with abutment	0.0170	-	0.0022	0.0044

**Table 4.** Manning's coefficients determined with automatic calibration ignoring theoretical intervals

	Manning's Coefficient (s/m <sup>1/3</sup> )		Error (m)	
	Steel/Glass	Wood	RMSE	Max. Residual
Flatbed channel	0.0155	-	0.0007	0.0018
Channel with sill	0.0050	0.05	0.0097	0.0187
Channel with abutment	0.0151	-	0.001	0.0022

**Table 5.** Boundary conditions

Boundary Conditions	Minimum Inflow		Medium Inflow		Maximum Inflow	
	Inlet BC (m <sup>3</sup> /s)	Outlet BC (m)	Inlet BC (m <sup>3</sup> /s)	Outlet BC (m)	Inlet BC (m <sup>3</sup> /s)	Outlet BC (m)
Flatbed channel	0.031	0.074	0.073	0.120	0.101	0.144
Channel with sill	0.041	0.035	0.070	0.055	0.108	0.078
Channel with abutment	0.040	0.086	0.064	0.112	0.100	0.140

**Table 6.** Final Manning's roughness coefficients

Material	Manning's roughness coefficient (s/m <sup>1/3</sup> )
Steel/Glass	0.017
Wood (sill)	0.014

546

547

548 FIGURE CAPTIONS

549 **Fig. 1** Initial flatbed channel

550 **Fig. 2** Crack geometry

551 **Fig. 3** First configuration - Positions of geometric and water depth surveys

552 **Fig. 4** Second configuration – Flow over a triangular sill

553 **Fig. 5** Second configuration - Sectional view

554 **Fig. 6** Second configuration - Positions of geometric and water depth surveys

555 **Fig. 7** Third configuration – Flow around a triangular abutment

556 **Fig. 8** Third configuration – Plan view

557 **Fig. 9** Third configuration - Positions of geometric and water depth surveys

558 **Fig. 10** Sensor on the sliding system

559 **Fig. 11** Comparison of the theoretical and step methods for calculating Manning's coefficients in  
560 the initial flatbed channel

561 **Fig. 12** Automatic calibration with PEST – From Lavoie and Mahdi (2016)

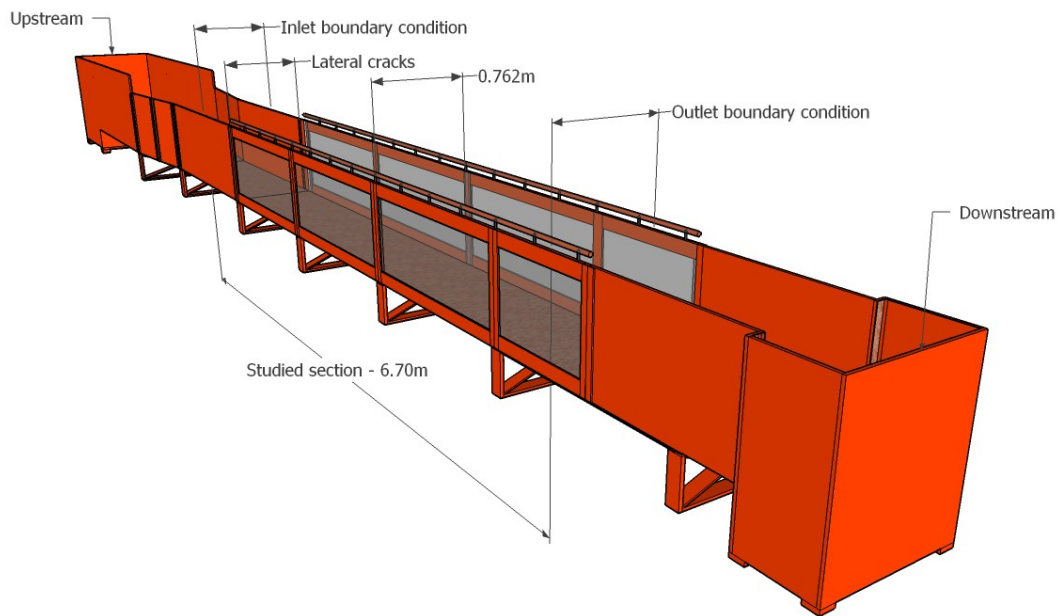
562 **Fig. 13a** Mesh of the initial flatbed channel

563 **Fig. 13b** Mesh of the channel with the triangular sill

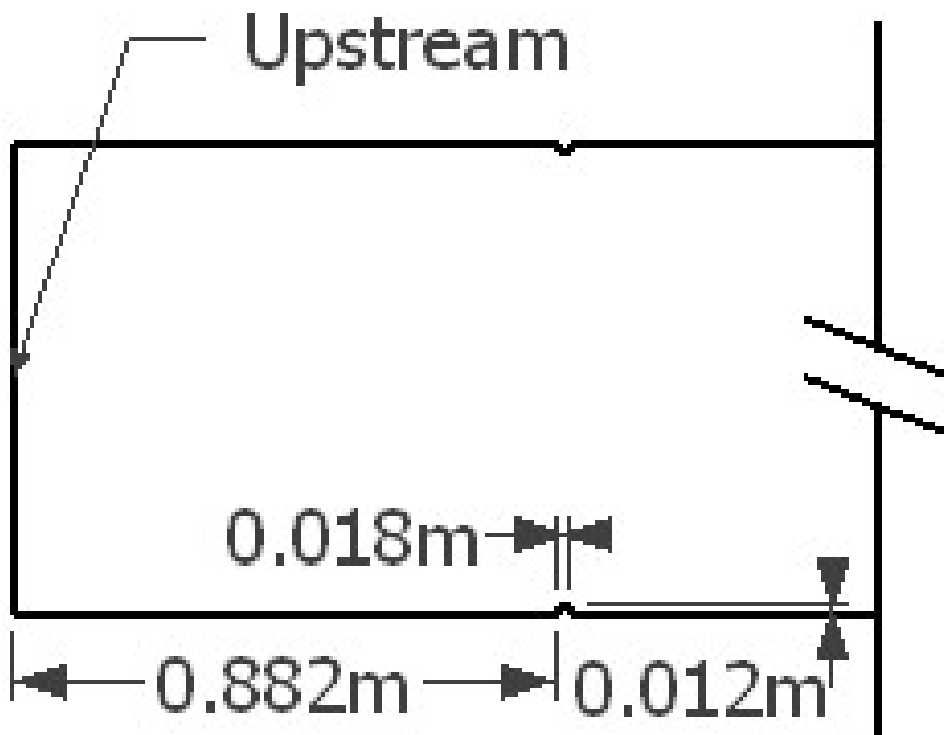
564 **Fig. 13c** Mesh of the channel with the triangular abutment

565 **Fig. 14** Comparison of water depth RMSEs calculated using SRH-2D for the three calibration  
566 methods

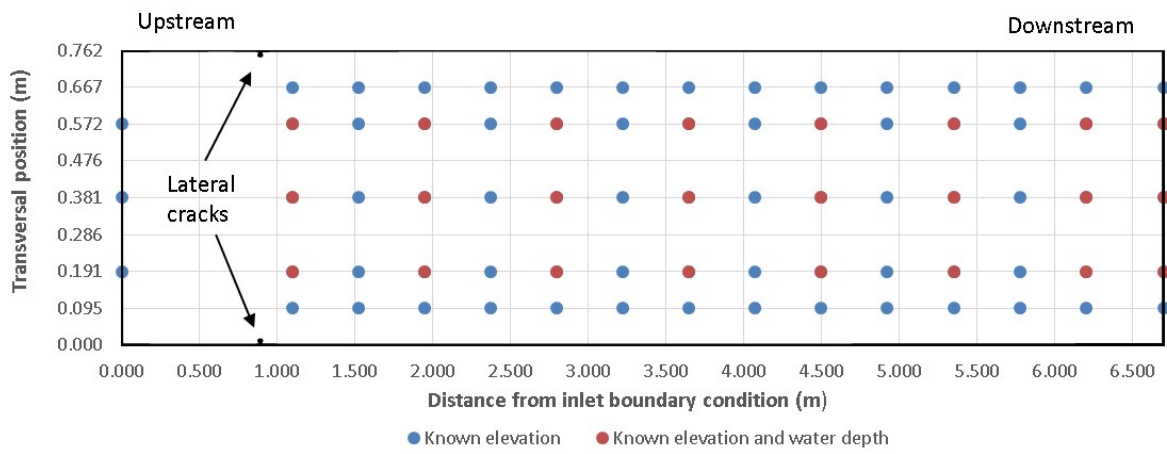
567



568  
569 Fig.1



570 Fig.2



571

572

Fig. 3

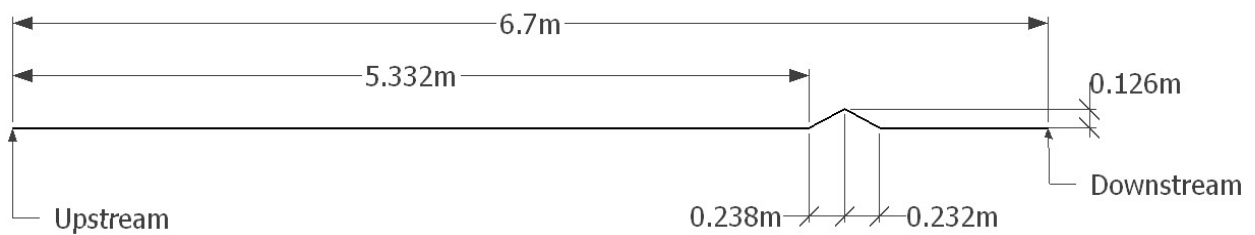


573

574

Fig. 4

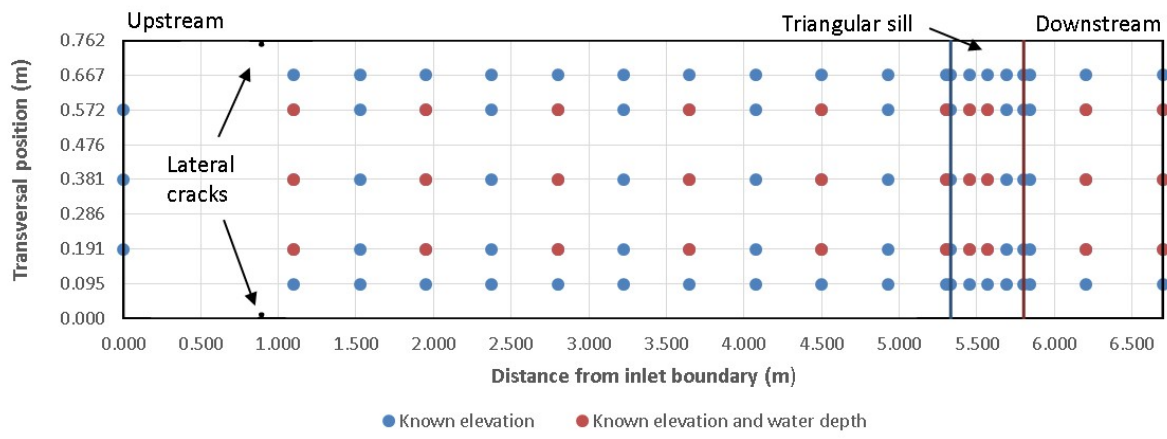
575



576

577

Fig. 5



578

579

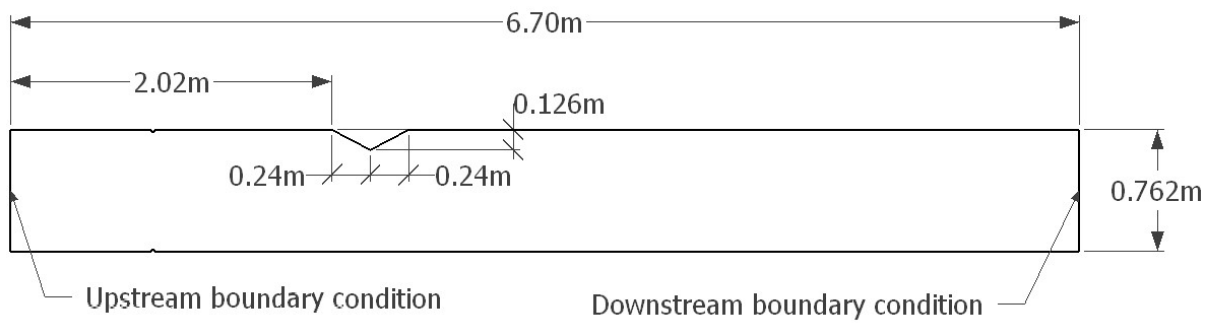
Fig. 6



580

581

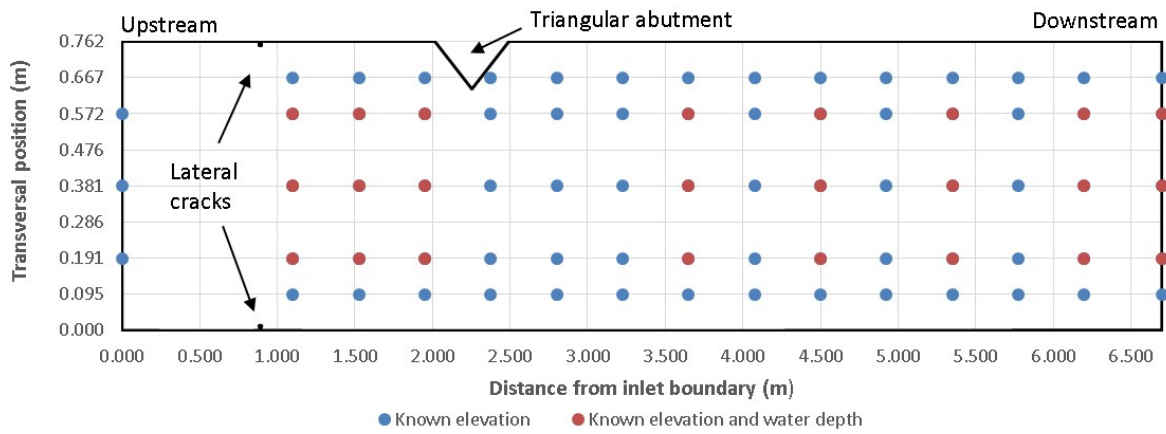
Fig. 7



582

583 Fig. 8

584



585

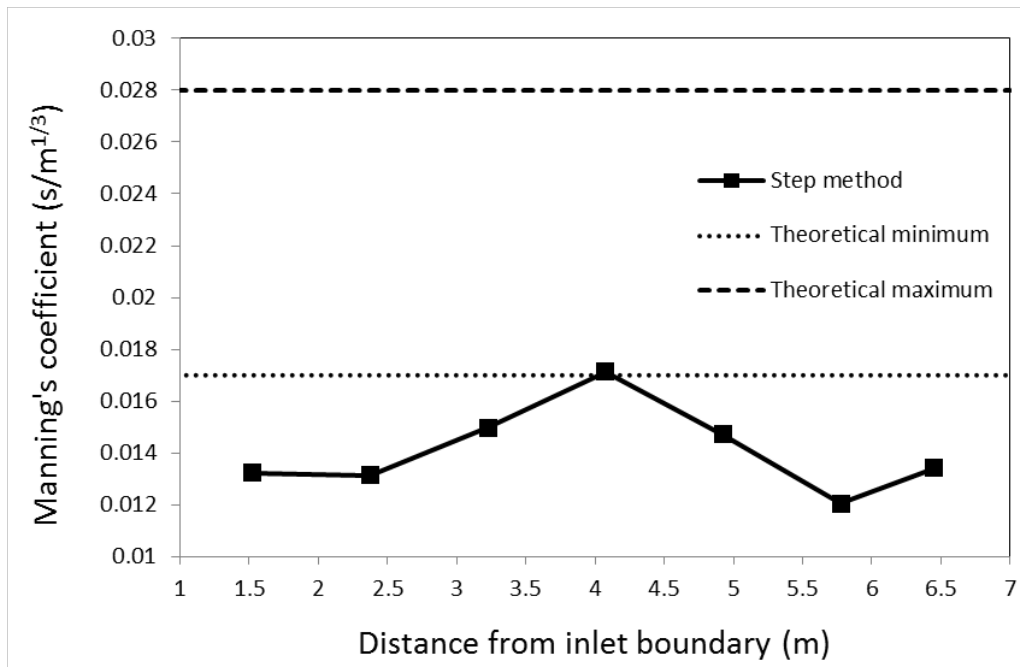
586 Fig. 9

587

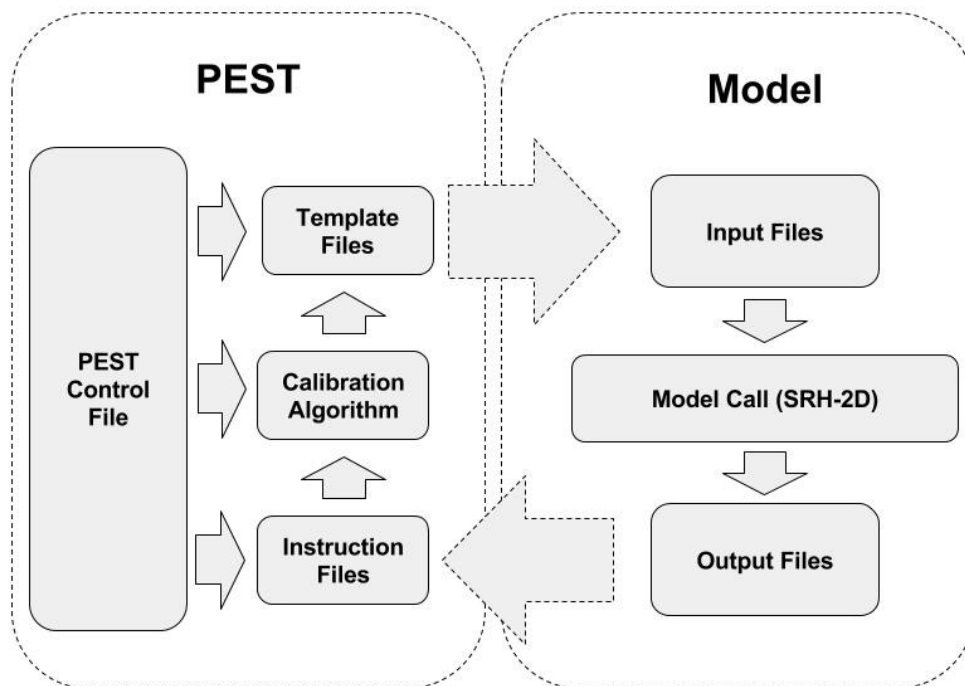


588

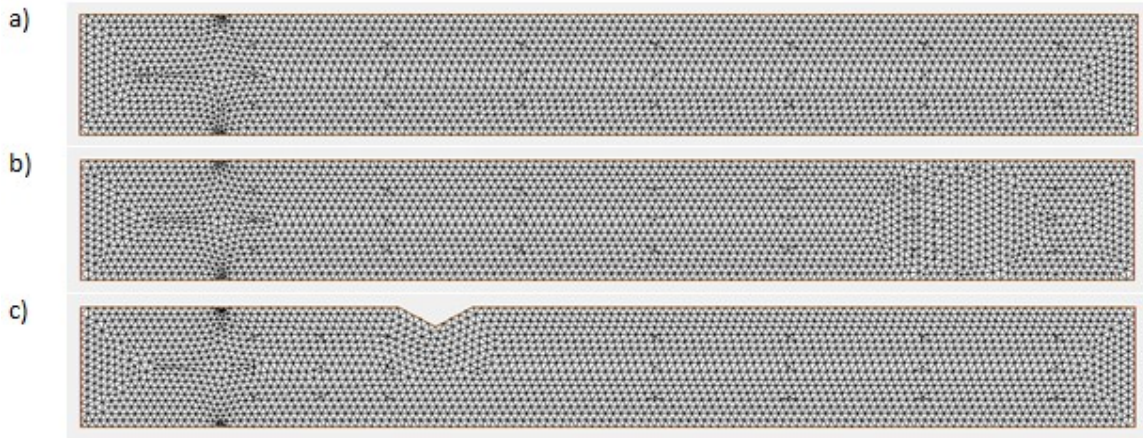
589 Fig. 10



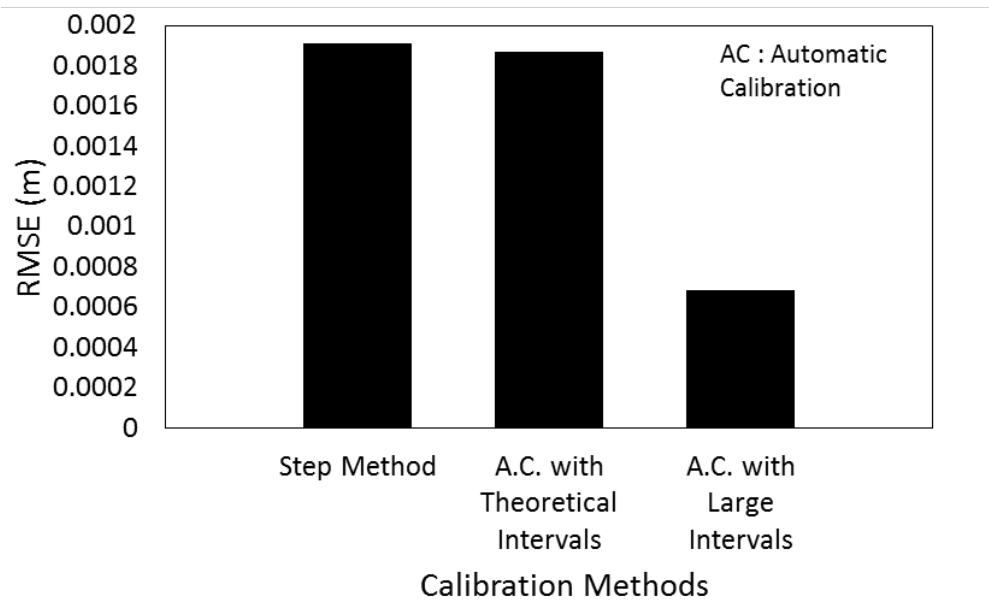
590  
591 Fig. 11  
592



593  
594 Fig. 12



595  
596 Fig. 13  
597



598  
599 Fig. 14  
600